Title

Controllable synthesis of hierarchical CuS/ZnS hetero-nanowires as high-performance visible-light photocatalysts

Journal

RSC Advances, 6(111)

ISSN

2046-2069

Authors

Feng, Caihong
Meng, Xianpu
Song, Xiaolu
et al.

Publication Date

2016

DOI

10.1039/c6ra20306j

Peer reviewed

Controllable Synthesis of Hierarchical CuS/ZnS Hetero-nanowires as High-Performance Visible-Light Photocatalyst

Caihong Feng,[a,b] Xianpu Meng,[a] Xiaolu Song,[c] Xueting Feng,[a] Yun Zhao,[a] and Gao Liu*[b]*

[a]School of Chemical Engineering and the Environmental, Beijing Institute of Technology, Beijing 100081, China

[b]Lawrence Berkeley National Laboratory, 1 Cyclotron Road, MS 70R108B, Berkeley, California 94720, United States

[c]Fengcheng Field Operation District，Xinjiang Oilfield Company，PetroChina

Abstract

Novel hierarchical CuS/ZnS hetero-nanowires were designed and successfully synthesized through a template-free chemical solution method with a mixed solvent of dimethyl sulfoxide and ethylene glycol. The precursors of CuS and the molar ratio of Cu:Zn, play a crucial role in controlling the morphology of the CuS/ZnS heterostructure. The precursors of CuS serve both as a source material for chemical transformation to CuS and as sacrificial templates for the growing of ZnS nanosheets by adding zinc (II) ions, finally forming ZnS/CuS hierarchical nanomaterial with p-n heterojunctions. The as-prepared samples were examined by X-ray diffraction, X-ray

photoelectron spectroscopy, scanning electron microscopy, transmission electron microscopy, UV-visible diffuse reflectance spectrum and Brunauer-Emmett-Teller measurement. Photocatalytic activities for methylene blue are investigated under visible-light irradiation and appreciably increased photocatalytic activity compared to individual counterparts is achieved by hierarchical CuS/ZnS hetero-nanowires. The p-n heterojunction, one-dimensional nanostructures and large specific surface area are responsible for the improved photocatalytic activities.

1. INTRODUCTION

The emerging energy crisis and environmental pollution have inspired the studies about energy conversion and environmental remediation. Considerable efforts have been devoted to design and fabricate semiconductor nanostructures with well-defined structures. They have unique size-dependent physical and chemical properties and have promising applications for energy conversion and environment remediation, such as sensors, nonlinear optical devices, solar cells, especially photocatalytic filed.[1-5] Expanding the light-harvesting range and suppressing the quick recombination of photo generated charge have paramount significance in the field photocatalysis.[6-8] To move toward this goal, engineering hetero-nanostructures by combination a relatively wide band gap semiconductor with some narrow band gap semiconductors is one of the most promising ways to achieve superior performances in wide range of applications. For examples, Zhang et al. prepared In_2S_3/TiO_2 hierarchical heterostructures, which showed a higher visible light photocatalytic activity than single TiO_2 or In_2S_3.[9] Kumar et al. enhanced the visible-light driven photocatalyst of $NaNbO_3$ by using $NaNbO_3$/CdS core/shell heterostructures.[10] In this context, it is feasible to form a coupled photocatalyst, which not only allows a broader range of solar light absorption, but also significantly promotes the separation of photogenerated charge carriers, thereby improves the photocatalytic efficiency.[11-12]

In recent years, nanostructured transition-metal sulfide semiconductors, including ZnS,[13] CdS,[14] MoS_2,[15] WS_2[16] and CuS[17] are generally viewed as excellent candidates for photocatalysts, due to their superior surface chemical/electronic properties. Among them, ZnS and CuS are considered to be promising because of their low cost and no secondary pollution.[18-19] ZnS, an important II (B)-VI (A) semiconductor with a wide band gap

(about 3.7 eV), has been widely investigated owing to its relatively tunable electric and optical properties, which offers ZnS good photocatalytic activity.[20-22] However, ZnS can only response for the absorption of ultraviolet (UV) irradiation, which greatly restricts its practical applications.[23] Another enduring impediment in the photocatalysis domain is the rapid recombination of photoinduced charge carriers.[24] Hence, it is highly desirable to design a photocatalyst with visible light activity and suppress charge carrier recombination to improve the photocatalytic efficiency. In view of this, the composites of ZnS/CuS with various morphologies including ZnS/CuS nanoflowers[25], nanosheets[26], and microspheres[27] were prepared and showed a better photocatalytic performance than the single component. The reason accounting for the remarkably enhanced photocatalytic efficiency is the interfacial charge transfer (IFCT) and extensive absorption range origin of the heterostructures of the composites. To the best of our knowledge, most of the reported ZnS/CuS composites were synthesized through ion-exchange method due to the different solubility product (Ksp) of ZnS (1.6×10^{-24}) and CuS (6.3×10^{-36}), so the as-prepared ZnS/CuS core/shell composites normally have a core of ZnS and a shell of CuS.[28] It is well known that CuS is susceptible to photocorrosion.[29] To some degree, it influences its cycling performance. And in this regard, a CuS/ZnS core/shell heterostructure may passivate the trap states of CuS and restrain the photocorrosion. However, there are few reports on the composite about CuS/ZnS core/shell structure. In addition, most reported ZnS/CuS materials are spheres and flowerlike, which are easily congregated under the photodegradation, and this may weaken the light harvesting. Though, ZnS/CuS composites with different morphologies have been prepared, the preparation of CuS/ZnS core/shell structure with 1D morphology is still a challenge. The construction of 1D heterostructures provides a feasible path in electronic conduction along the axial direction and has new prospect to obtain high photocatalytic performance. Therefore, systematic tuning of the composition, size, shape, and phase matched to metal sulfide semiconductor or heterojunctions can tune physical behavior of CuS/ZnS.

In this work, we present the fabrication of hierarchical CuS/ZnS hetero-nanowires with different ratios of CuS:ZnS via a solution-based and template-free method in a mixed solvent of dimethyl sulfoxide and ethylene glycol. CuS/ZnS hetero-nanowires were extensively characterized and investigated. The factors influencing formation of CuS/ZnS hetero-nanowires were discussed and the photocatalytic activities of as prepared

CuS/ZnS hetero-nanowires under visible light irradiation were investigated by degradation of MB solutions. A possible photocatalytic mechanism of CuS/ZnS hetero-nanowires is proposed as well. An in-depth study of mechanism suggesting the formation of heterojunctions attribute to the enhanced photocatalytic activity.

2. EXPERIMENT SECTION

2.1 Materials

Copper (II) nitratetrihydrate ($Cu(NO_3)_2 \cdot 3H_2O$), zinc (II) nitrate hexahydrate ($Zn(NO_3)_2 \cdot 6H_2O$), thiourea (CH_4N_2S), hydrogen peroxide (H_2O_2, 30%), ethylene glycol (EG), methylene blue (MB) and dimethyl sulfoxide (DMSO) were purchased from Beijing Chemical Reagent Company. All the above reagents were analytical grade and used without further purification.

2.2 Synthesis of CuS/ZnS Hetero-nanowires

The CuS nanowire precursors were prepared as our previous work[30] and served as a scaffold for the fabrication of CuS/ZnS hetero-nanowires. In a typical process, 2 mmol $Cu(NO_3)_2 \cdot 3H_2O$ was dissolved in the mixed solvent (120 mL) with a volume ratio of $V_{DMSO}/V_{EG}=1/3$ under stirring in a three-neck flask at room temperature. Then the flask was placed into oil bath and heated at 145 °C and maintained for 4 hours under nitrogen ambience to generate green-yellow CuS nanowire precursors. Afterwards, 1 mmol $Zn(NO_3)_2 \cdot 6H_2O$ dissolved in mixed solvent was dropped into the solution and stirred gently for 30 minutes. At last, 10 mL of mixed solution containing 0.685 g of thiourea (9 mmol) was added to the solution drop by drop through a syringe under vigorous stirring and reacted for another 2 hours. The final products labeled as $CZ_{0.5}$ were centrifuged and washed several times by distilled water and ethanol and dried in a vacuum drying oven at 60 °C for further characterization. $CZ_{0.2}$ was synthesized under the same condition except that the different molar ratio of CuS to ZnS is 0.2. The schematic illustrations for the process to synthesize CuS/ZnS heterostructures are shown in Scheme 1. For comparison, pristine CuS nanowires and ZnS were prepared by a similar process in the absence of $Zn(NO_3)_2 \cdot 6H_2O$ and $Cu(NO_3)_2 \cdot 3H_2O$, respectively.

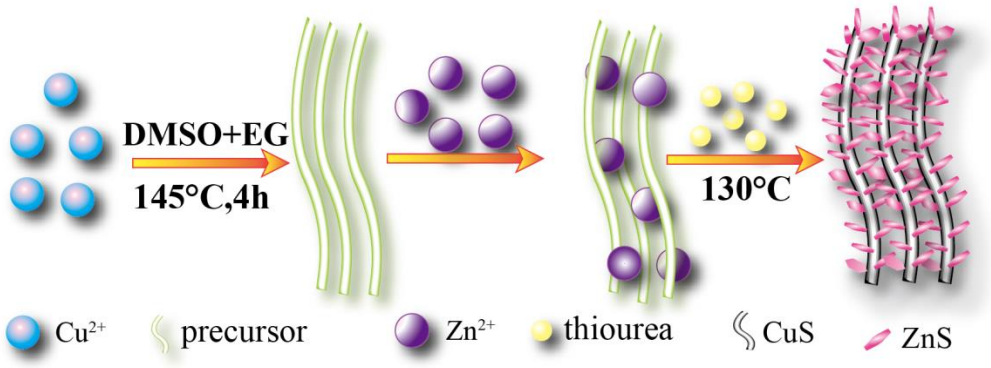

Scheme 1. Schematic illustration of the synthetic route of the CuS/ZnS hetero-nanowires.

2.3 Characterization

The phase compositions and crystal structures of the as-prepared samples were characterized using a Philips X'Pert Pro Multipurpose X-ray diffraction (XRD) analysis with Cu Kα radiation at 40 kV and 40 mA, scanning ranges from 10° to 80° at a scan rate of 0.02° per step. The valence types of samples were detected by PHI QUANTERA-II SXM X-ray photoelectron spectroscopy (XPS). The morphologies of the samples were characterized by scanning electron microscopy (SEM) on a JEOL JSM-7500F microscope operated at 25 kV and transmission electron microscopy (TEM) on a JEOL JEM-2100F field emission microscope at 100 kV. The UV-visible diffuse reflectance spectrum (UV-vis DRS) of samples were recorded from 200 nm to 800 nm on U-3900, Hitachi, and $BaSO_4$ was used as a reflectance standard. Nitrogen adsorption–desorption isotherms, specific surface area was analyzed by using Quanta autosorb iQ system and the pore size diatribution was determined by the Barrett-Joyner-Halenda (BJH) method.

2.4 Photocatalytic Experiments

Methylene blue, one of familiar and typical dyes containing N-group, was carried out to evaluate the photocatalytic performance of as-prepared samples. The experiment was performed at room temperature and the specific process was as follows: First, 20 mg as-prepared catalyst was dispersed into 200 mL MB solution with the concentration of 10 mg/L under vigorously stirred for 1h in the dark to establish the adsorption/desorption equilibrium. Then, 200 μL H_2O_2 was put in the solution and a 300 W xenon lamp with a UV-cut off filter (≥400 nm) was placed 62 cm away from the solution and employed as a visible-light

spectrophotometer to trigger the photocatalytic reaction. Every 10 minutes, 3 mL solution was taken out and filtered with a 0.22 μm membrane. The concentration of MB was detected by an ultraviolet and visible spectrophotometer. The characteristic absorption peak of MB at 664 nm was chosen to monitor the whole photodegradation process.

3. RESULTS AND DISCUSSION

XRD analysis was applied to determine the ingredient and crystalline structures of as prepared samples. The patterns of CuS, ZnS and CuS/ZnS composites with different ratio of ZnS are shown in Figure 1. All the diffraction peaks in Figure 1a can match well with the hexagonal phase of CuS (JCPDS No. 06 0464) and the diffraction peaks of as-prepared ZnS in Figure 1d can be indexed to the standard peaks of hexagonal phase ZnS (JCPDS No. 36-1450). The diffraction peaks of CuS/ZnS composites in Figure 1b, c contribute to CuS and ZnS. The observed peaks at 2θ= 27.2°, 27.7°, 29.4°, 32.0°, 33.0°, 48.2°, 52.8°, and 59.3° can be indexed to the (100), (101), (102), (103), (006), (110), (108), and (116) reflections of CuS respectively. The diffraction peaks at 28.5°, 30.5°, 47.5°, 56.4° can be indexed to the (002) (101) (110) (112) reflections of ZnS hexagonal phase. No new phases can be detected in the CuS/ZnS composites. A careful examination of the XRD patterns reveals that the intensities of ZnS diffraction peaks are gradually strengthened with the increasing of the ratio of ZnS:CuS, which is consist with the content of ZnS as we designed.

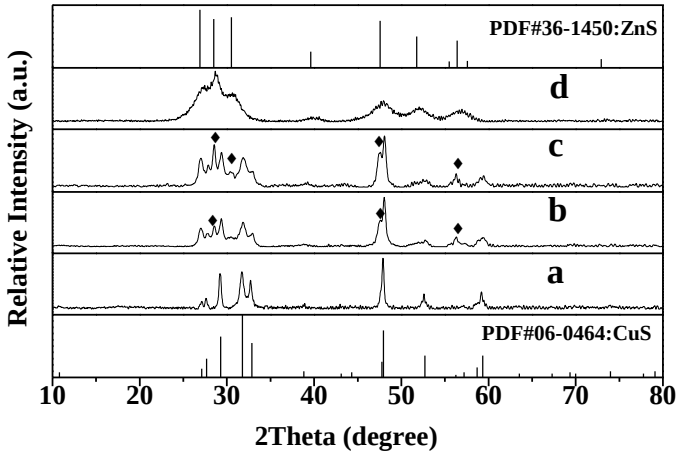

Figure 1. XRD patterns of (a) CuS, (b) CZ0.2, (c) CZ0.5, and (d) ZnS.

SEM and TEM are used to characterize the morphologies of as-prepared samples. The typical SEM image in Figure 2a displays that the product of $CZ_{0.5}$ is composed of nanowires with uniform diameter of about 100 nm and lengths up to several micrometers. More details of $CZ_{0.5}$ nanowires are revealed in the high magnification image and shown in the inset. Compared with precursors of CuS and pristine CuS nanowires (Supporting Information, Figure S1a,b), $CZ_{0.5}$ keeps a similar 1D nanostructure as that of the CuS precursors and pristine CuS nanowires, but instead of original smooth surface, there are many uniform sheets inserting on the surface of the nanowires and forming a fluffy hierarchical nanostructure. 1D $CZ_{0.5}$ hetero-nanowires were further investigated by TEM and HRTEM and shown in Figure 2b, c. It reveals that many nanosheets vertically insert on the nanowires, which are consistent with the SEM images. As shown in the high-resolution TEM image in Figure 2c, the lattice fringes can be obviously observed, suggesting the well-defined crystal structure. The lattice spacing of 0.19 nm corresponds to the (110) plane of ZnS and the lattice spacing of 0.28 nm corresponds to the (103) plane of CuS respectively. The Selected Area Electron Diffraction (SAED) pattern of $CZ_{0.5}$ shows the well-defined diffraction rings in Figure 2d. The rings can be readily indexed to the (103), (108) planes of CuS and (102), (110) planes of ZnS, which are consistent with the XRD results. These results imply that ZnS and CuS could form a p-n heterojunction instead of physical mixture. Both the 1D structure and heterojunctions are believed to improve the transfer of photogenerated electrons and holes between ZnS and CuS, enhance the charge separation and benefit for the catalysis performance of material, which will be particularly discussed afterwards.[31]

Controlled experiments were performed to understand the influence of the precursor on the formation of CuS/ZnS hetero-nanowires. When adding $Zn(NO_3)_2 \cdot 6H_2O$, $Cu(NO_3)_2 \cdot 3H_2O$ and solvent together at the beginning, the morphology of the product is flower-like structure instead of nanowires (Supporting Information, Figure S1c). The ZnS nanomaterials prepared in the absence of $Cu(NO_3)_2 \cdot 3H_2O$ bears sphere morphology with the uniform size about 200 nm (Supporting Information, Figure S1d). It proves that the precursor serves as a scaffold for the inserting of ZnS nanosheets. It should be pointed that Zn:Cu molar ratio also strongly affected the nucleation and growth rate, and subsequently induced various morphologies. Compared the image of $CZ_{0.5}$ and $CZ_{0.2}$ (Supporting Information, Figure S1e), both of them are keeping the 1D nanowires structures and there

are more sheets inserting on the surface of the $CZ_{0.5}$ than that of $CZ_{0.2}$, which provides more interconnection. When the ratio of Zn:Cu is up to 0.7, the morphology changes from nanowires to flower-like multilevel structure (Supporting Information, Figure S1f). The aforementioned results confirm the feasibility of our design approach and the importance of CuS precursors and the ratio of Zn^{2+}.

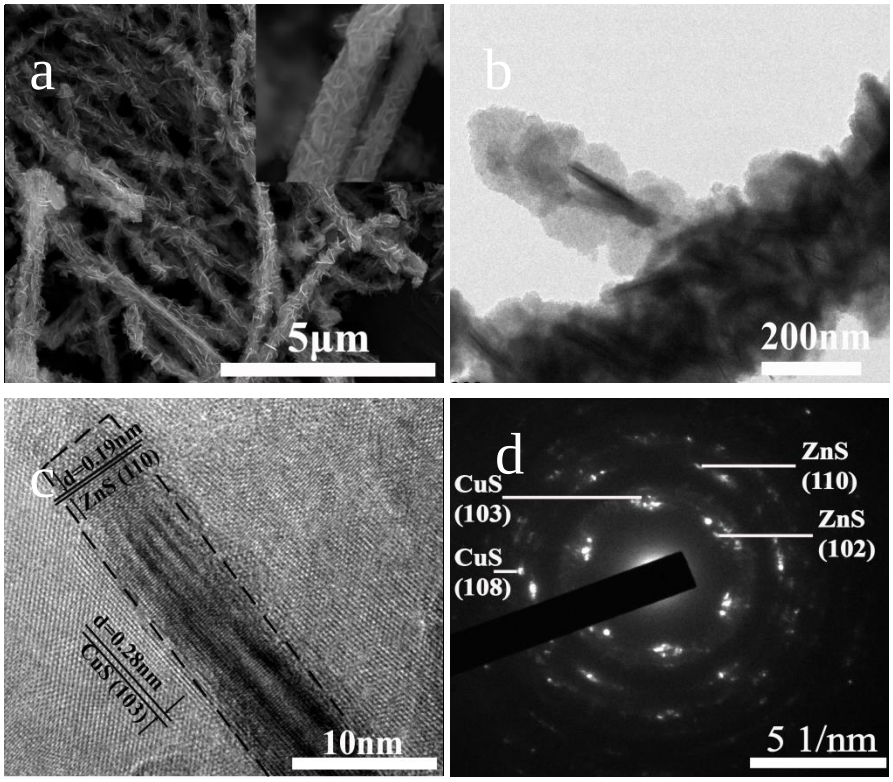

Figure 2. (a) SEM, (b) TEM, (c) HRTEM image and (d) SAED patterns of samples $CZ_{0.5}$.

XPS was used to illuminate the chemical states of the elements in the prepared samples. Figure 3a exhibits the XPS survey spectrum of the sample $CZ_{0.5}$. From the survey spectrum, the peaks of Zn 2p, Cu 2p, S 2p, C 1s and O 1s can be easily observed. The peak of O and C should attribute to the CO_2, O_2 and H_2O absorbed on the surface of the sample.[32] Figure 3 b-d show the high-resolution XPS spectra of Zn 2p, Cu 2p, S 2p. As shown in the Figure 3b, the binding energy peaks of Cu $2p_{3/2}$ and Cu $2p_{1/2}$ at 932.8 eV and 952.6 eV are corresponding to the typical values of Cu^{2+} in CuS and agrees with the literature.[33] In addition, there are several weak shake-up satellite peaks at around 943.5 eV, indicating the paramagnetic chemical state of Cu^{2+}.[34-35] Furthermore, the excellent symmetry of the each peak of Cu 2p peaks clearly implies purity of Cu^{2+}. In the Figure 3c, the two

strong and symmetrical peaks at 1044.9 eV and 1021.9 eV are ascribe to the binding energies of Zn $2p_{3/2}$ and Zn $2p_{1/2}$, respectively, indicating the presence of pure Zn^{2+}.[36] Figure 3d shows the S 2p XPS inspection of the sample. The peaks at 161.9 eV and 162.8 eV ascribe to S^{2-} ($2p_{3/2}$ and $2p_{1/2}$) and indicate the presence of composite metal sulfides[37]. In general, it is rational to infer that the sample is composed of CuS and ZnS. It is consistent with the XRD result.

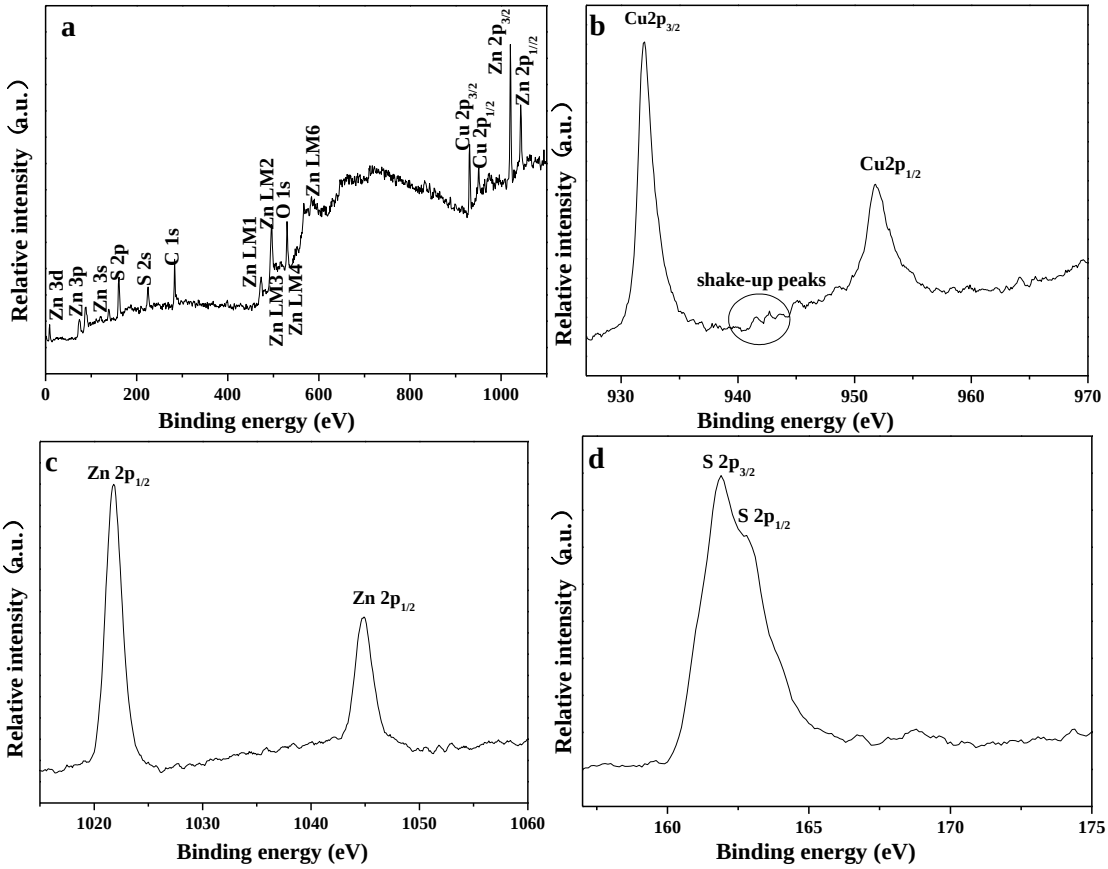

Figure 3. The XPS spectra of the CZ0.5: (a) survey spectra, (b) Cu 2p region, (c) Zn 2p region and (d) S 2p region.

The nitrogen adsorption-desorption measurements were performed to evaluate the specific surface area and pore structure of samples. As shown in Figure 4, the isotherms profile display irreversible types IV (the IUPAC classification), indicating the mesoporous structure of as-prepared samples.[38] The hysteresis loops in curve of $CZ_{0.2}$ and $CZ_{0.5}$ classified as type H3 in the isotherms associates with slit-like loops and matches well with the CuS/ZnS secondary structure.[39] The adsorbed nitrogen volume surges where relative pressure close to unity, implying the existence of large interconnected voids or void space within the nanowires, agreed with

nanosheets inserting on the nanowires.[39] The inset depicts a pore size distribution ranging from 2 to 30nm, which is known to be optimal for catalyst applications and further indicates the presence of mesoporous structure. The BET specific surface areas and pore volumes of all the samples are summarized in Table 1. As shown in Table 1, $CZ_{0.2}$ and $CZ_{0.5}$ exhibit higher BET surface areas and pore volume than that of CuS nanowires. The increased specific surface areas of CuS/ZnS hetero-nanowire can be attributed to the formation of CuS/ZnS hierarchical structure. The higher specific surface area and pore volume can offer more diffusion paths for the related molecule transport and increased reactive sites between the electronic receptor and the supplier, which can greatly improve the photocatalytic performance of CuS/ZnS.[40]

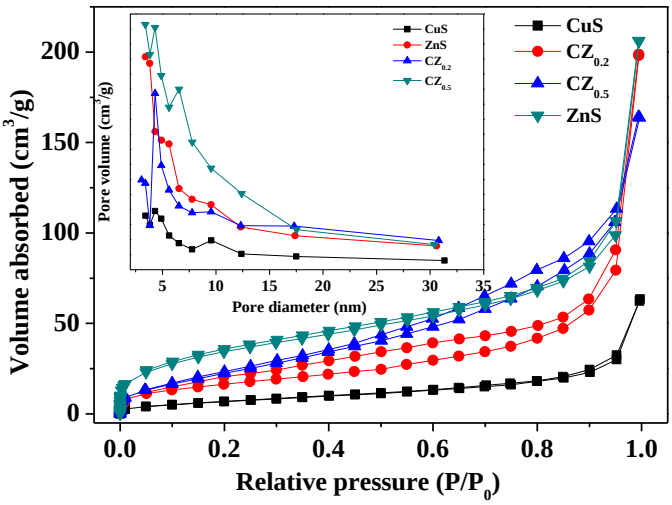

Figure 4. The nitrogen adsorption-desorption isotherms and corresponding pore size distribution curves of CuS, ZnS, $CZ_{0.2}$, and $CZ_{0.5}$.

Table 1. BET surface areas and pore volumes of the prepared samples.

no.	composition	morphology	S_{BET} (m^2g^{-1})	pore volume (cm^3g^{-1})
1	CuS	nanowires	27.711	0.09817
2	ZnS	sphere	123.3	0.319
3	$CZ_{0.2}$	hetero-nanowires	66.439	0.2368
4	$CZ_{0.5}$	hetero-nanowires	98.507	0.2531

Figure 5a shows the comparison of photocatalytic activity of CuS, ZnS, $CZ_{0.5}$ and the mixture of ZnS and CuS. It can be clearly observed that, under the same visible light irradiation, the UV-active ZnS shows a negligible photocatalytic activity, and only 22% MB was degraded in 60 min, which should be attribute to the action of H_2O_2. The degradation rate of CuS is faster than ZnS and the reason is that CuS is a narrow gap semiconductor responding to visible light. In fact, $CZ_{0.5}$ shows a substantial strength in both degradation rate and efficiency. It exhibits an amazing efficiency (98%) of visible light photocatalysis in 60 min for $CZ_{0.5}$, higher than that of CuS (84%). It is well known that the morphology has influence on the catalytic performance. The sample of $CZ_{0.5}$ with lager specific surface area offers the most react sites, which accelerates the degradation. Furthermore, to understand the role of heterostructure of CuS/ZnS, the photocatalysis experiment of physical mixture of CuS and ZnS (with the ratio CuS:ZnS=1:0.5) was conducted. The efficiency of mixture (only 66%) is lower than that of $CZ_{0.5}$ in 60 min, which demonstrate the physical mixture without heterojunctions couldn't improve the photocatalytic performance. Figure 5b shows the evolution of UV-vis absorption spectra of MB under visible irradiation with the presence of H_2O_2 and $CZ_{0.5}$. As can be seen, the characteristic peak at 664 nm weakened gradually and no other peak appeared, which indicated that the degradation of MB molecular was a direct cleavage of the aromatic ring not simple photooxidative N-demethylation.[41] The high photodegradation efficiency of CuS/ZnS hetero-nanowires catalysts can be explained by p-n heterojunctions that induce the efficient separation of photogenerated electron-hole pairs and 1D structure that are benefical for the diffusion of reactant molecular to the active sites. [25, 40]

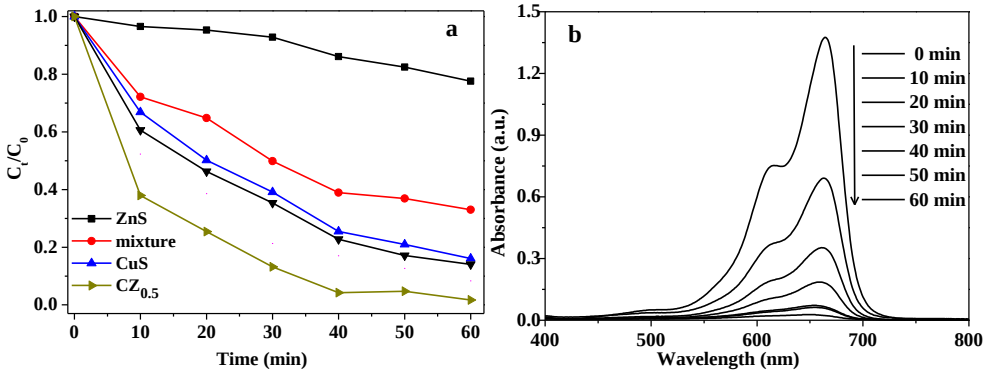

Figure 5. (a) Comparison of photocatalytic efficiency of samples for the degradation of MB under visible light; (b) Photocatalytic degradation of MB in the presence of $CZ_{0.5}$ and 200μL H_2O_2.

The cycling degradation test was performed to detect the stability of material CuS/ZnS hetero-nanowires. As shown in Figure 6, the catalyst $CZ_{0.5}$ did not exhibit any significant loss of activity, after 5 recycles for degradation of MB under the same condition. In details, the efficiency can also be up to 93%, and the efficiency reduction should be according to the loss of the catalyst during the progress of taking sample and centrifugation. The result confirmed that the 1D hetero-nanowires were not deactivated during the photocatalytic oxidation and the CuS/ZnS core/shell structure suppressed the photocorrosion successfully.

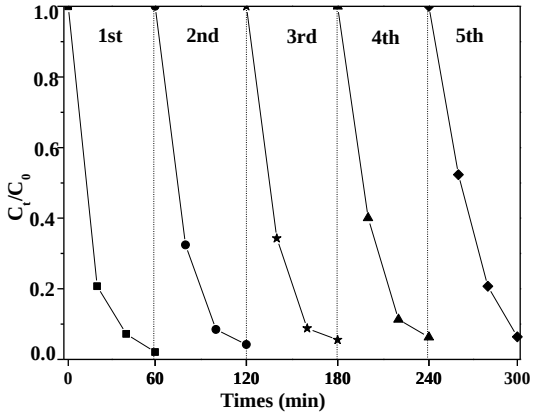

Figure 6. Cycling degradation efficiency for the $CZ_{0.5.}$

To further explain the different photocatalytic performance of as-prepared CuS, ZnS and CuS/ZnS hetero-nanowires, UV-vis DRS studies were measured, and the results are presented in Figure 7. As shown in the pattern of ZnS, there is an absorption band in UV range and no absorption in the visible, which attributes to the wide forbidden band that makes transition of the electron from valence band to conduction band hard.[42] The relatively absorption at the wavelength of 320 nm is attributed to the intrinsic band gap absorption of ZnS, and the band gap energy is calculated to be 3.9 eV according to the Tauc approach (Supporting Information, Figure S2a). However, CuS have a widen absorption range from 200 to 800 nm, especially a strong absorption in 700-800 nm assigned to the d-d transition of Cu^{2+}.[26, 43-45] The relevant band gap is 1.55 eV (Supporting Information, Figure S2b), which agrees with the reported value.[27] Compared with ZnS, CuS, and the mixture of ZnS and CuS, the UV-vis DRS profile of $CZ_{0.5}$ hetero-nanowires present a combination of the spectral features of ZnS and CuS alone, and conveys a broadened absorption range, a shift in the absorption onset to longer wavelengths, as well as the intensity increasing. It demonstrates that the $CZ_{0.5}$ hetero-nanowires possess both

UV and visible light response, which indicates an enhanced photocatalytic performance. The longer wavelength absorption and observed broadening of the absorption spectra should be scrutinized in terms of the nanowires hierarchical structure and the formation of p-n heterojunctions. It has been reported by Hong et al. and Zhang et al. that the IFCT in the heteronanostructures of CuS/ZnS nanoflowers spheres and CuS/ZnS porous nanosheets is beneficial for the photogenerated charge separation and then enhance visible light photocatalytic activity.[26, 46] Li et al. also reported that photo-generated holes from the valence band (VB) of CdS transferred to the defect states of the heterojunction, interfacial $Zn_{1-x}Cd_xS$ layer, because of the lower holes acceptors band, thus enhanced the charge separation and transport efficiency.[47] The responding $CZ_{0.5}$ band gap calculations (Supporting Information, Figure S2c) gives the band gap 1.86 eV for $CZ_{0.5,}$ which is larger than that of CuS and smaller than ZnS. The appropriate band gap may play a transition role in boosting the separation of electrons and holes.

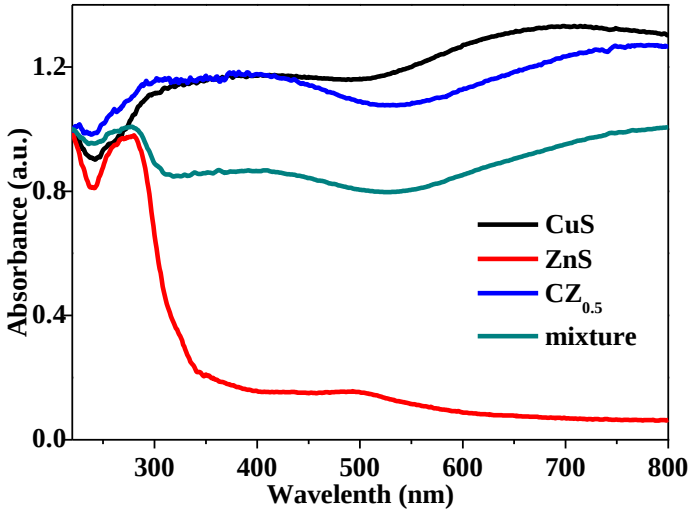

Figure 7. UV-vis DRS absorbance spectra of as-prepared CuS, ZnS, mixture and $CZ_{0.5}$ hetero-nanowires.

Based on the results, the improved photocatalytic performance should be ascribed to the follow aspects: First, the nanosheets inserted on the nanowires increase the specific surface area of materials, which increases the active site in the photodegradation process. Second, the p-n heterojunctions facilitate the interfacial charge transfer and suppress the combination of holes and electrons. Third, the 1D structure is in favor of the electron transfer along the axial direction, accelerating the rate of electrochemical reaction processes. The possible photocatalytic mechanism of MB using CuS/ZnS hetero-nanowires as photocatalyst describes in Scheme 2.

The light penetrates through the bulk solution to reach the CuS surface. CuS as a visible light photo sensitizer can response to the visible light due to its suitable band gap energy, While the ZnS cannot response to the visible light because of the large forbidden band gap. The valence electron of CuS is excited by visible light and transits to its conduction band, and it forms holes at valence band at the same time. It is forbidden that the electrons and holes of CuS transfer to the corresponding conducted band and valence band of ZnS because of the type (I) structure. [48-49] But the electrons on the surface of CuS can be captured by the O_2 and form superoxide anion ($\cdot O_2^-$.) The $\cdot O_2^-$, with strong oxidizability, not only can degrade MB directly but also react with H_2O and generate $OH\cdot$ to degrade the MB indirectly. In addition, because of the existences of Zn vacancies on ZnS and interface, the holes on CuS transfer to the vacancies of ZnS and heterojunctions, as was reported by the related literature.[47] The transferred holes also engage in the photocatalysis process, which has been proved by the trapping experiment conducted by concerned investigators.[36, 48] As mentioned above, the electrons and holes delocalize in the broader space, which increases the stability of them and results in the separation of electrons and holes, improving the photocatalysis efficiency.

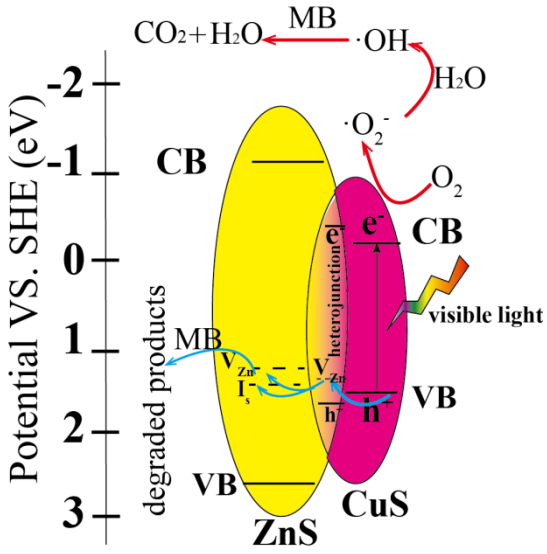

Scheme 2. The photocatalytic mechanisms of $CZ_{0.5}$.

CONCLUSIONS

In summary, we fabricated high performance 1D hierarchical CuS/ZnS hetero-nanowires with p-n junction using a chemical solution method. The precursors and Cu:Zn molar ratio played an important role in control of the morphology of products. The hetero-nanowires $CZ_{0.5}$ exhibited great photocatalytic degradation ability under visible light, and the MB molecules were almost degraded completely in 60 min. It is p-n heterojunctions, 1D nanoporous structure, and the larger specific surface area that account for the enhanced visible li,ght photocatalytic activity. In addition, the outer ZnS shell restrains the photocorrosion of inner CuS, improved the cycling performance. This chemical solution method is simple and efficient to synthesis the other dual metal sulfides core/shell structure, holding great promising.

ASSOCIATED CONTENT

Supporting Information

SEM image of the precursors, CuS, CuS/ZnS prepared at the condition of adding $Zn(NO_3)_2 \cdot 6H_2O$, $Cu(NO_3)_2 \cdot 3H_2O$ and solvent together, ZnS, $CZ_{0.2}$, and $CZ_{0.7}$; The band gap calculation of ZnS, CuS, and $CZ_{0.5.}$ This material is available free of charge via the Internet at http://pubs.acs.org.

AUTHOR INFORMATION

Corresponding Authors

*Y. Zhao. E-mail: zhaoyun@bit.edu.cn. Fax: +86 1068918979. Tel: +86 10 68918979.

*G. Liu. E-mail: gliu@lbl.gov. Fax: 00 510 4867207. Tel: 005104867303.

Notes

The authors declare no competing financial interest.

REFERENCES

1. Ansari, S. A.; Khan, M. M.; Ansari, M. O.; Cho, M. H., Nitrogen-doped titanium dioxide (N-doped TiO2) for visible light photocatalysis. *New J. Chem.* **2016,** *40* (4), 3000-3009.

2. Li, G.; Su, R.; Rao, J.; Wu, J.; Rudolf, P.; Blake, G. R.; de Groot, R. A.; Besenbacher, F.; Palstra, T. T. M., Band gap narrowing of SnS2superstructures with improved hydrogen production. *J. Mater. Chem. A* **2016,** *4* (1), 209-216.

3. Low, J.; Cao, S.; Yu, J.; Wageh, S., Two-dimensional layered composite photocatalysts. *Chemical communications* **2014,** *50* (74), 10768-77.

4. Varughese, G., Characterization and Optical Study on Zinc Sulphide Nanostructures Doped with Gadolinium Ions. *Materials Today: Proceedings* **2016,** *3* (2), 282-288.

5. Wang, T.; Meng, X.; Li, P.; Ouyang, S.; Chang, K.; Liu, G.; Mei, Z.; Ye, J., Photoreduction of CO2 over the well-crystallized ordered mesoporous TiO2 with the confined space effect. *Nano Energy* **2014,** *9*, 50-60.

6. Cheng, H.; Huang, B.; Dai, Y.; Qin, X.; Zhang, X., One-step synthesis of the nanostructured AgI/BiOI composites with highly enhanced visible-light photocatalytic performances. *Langmuir : the ACS journal of surfaces and colloids* **2010,** *26* (9), 6618-24.

7. Hu, Y.; Liu, Y.; Qian, H.; Li, Z.; Chen, J., Coating colloidal carbon spheres with CdS nanoparticles: microwave-assisted synthesis and enhanced photocatalytic activity. *Langmuir : the ACS journal of surfaces and colloids* **2010,** *26* (23), 18570-5.

8. Yu, K.; Yang, S.; Liu, C.; Chen, H.; Li, H.; Sun, C.; Boyd, S. A., Degradation of organic dyes via bismuth silver oxide initiated direct oxidation coupled with sodium bismuthate based visible light photocatalysis. *Environmental science & technology* **2012,** *46* (13), 7318-26.

9. Zhang, X.; Li, X.; Shao, C.; Li, J.; Zhang, M.; Zhang, P.; Wang, K.; Lu, N.; Liu, Y., One-dimensional hierarchical heterostructures of In(2)S(3) nanosheets on electrospun TiO(2) nanofibers with enhanced visible photocatalytic activity. *Journal of hazardous materials* **2013,** *260*, 892-900.

10. Kumar, S.; Khanchandani, S.; Thirumal, M.; Ganguli, A. K., Achieving enhanced visible-light-driven photocatalysis using type-II NaNbO3/CdS core/shell heterostructures. *ACS applied materials & interfaces* **2014,** *6* (15), 13221-33.

11. Yuan, Y.-P.; Ruan, L.-W.; Barber, J.; Joachim Loo, S. C.; Xue, C., Hetero-nanostructured suspended photocatalysts for solar-to-fuel conversion. *Energy Environ. Sci.* **2014,** *7* (12), 3934-3951.

12. Mayer, M. T.; Yongjing, L.; Guangbi, Y.; Dunwei, W., Forming heterojunctions at the nanoscale for improved photoelectrochemical water splitting by semiconductor materials: case studies on hematite. *Accounts of Chemical Research* **2013,** *46* (7), 1558-66.

13. Zhang, S., Preparation of controlled-shape ZnS microcrystals and photocatalytic property. *Ceramics International* **2014,** *40* (3), 4553-4557.

14. And, D. J.; Guo, L., A Novel Method for the Preparation of a Highly Stable and Active CdS Photocatalyst with a Special Surface Nanostructure. *Journal of Physical Chemistry B* **2006,** *110* (23), 11139-45.

15. Li, Y.; Li, Y.-L.; Araujo, C. M.; Luo, W.; Ahuja, R., Single-layer MoS2 as an efficient photocatalyst. *Catalysis Science & Technology* **2013,** *3* (9), 2214.

16. Sang, Y.; Zhao, Z.; Zhao, M.; Hao, P.; Leng, Y.; Liu, H., From UV to near-infrared, WS2 nanosheet: a novel photocatalyst for full solar light spectrum photodegradation. *Advanced materials* **2015,** *27* (2), 363-9.

17. Tanveer, M.; Cao, C.; Ali, Z.; Aslam, I.; Idrees, F.; Khan, W. S.; But, F. K.; Tahir, M.; Mahmood, N., Template free synthesis of CuS nanosheet-based hierarchical microspheres: an efficient natural light driven photocatalyst. *CrystEngComm* **2014,** *16* (24), 5290.

18. Leonard, D. P.; Pan, H.; Heagy, M. D., Photocatalyzed Reduction of Bicarbonate to Formate: Effect of ZnS Crystal Structure and Positive Hole Scavenger. *ACS applied materials & interfaces* **2015,** *7* (44), 24543-9.

19. Saranya, M.; Ramachandran, R.; Samuel, E. J. J.; Jeong, S. K.; Grace, A. N., Enhanced visible light photocatalytic reduction of organic pollutant and electrochemical properties of CuS catalyst. *Powder Technology* **2015,** *279*, 209-220.

20. Chen, F.; Cao, Y.; Jia, D.; Liu, A., Solid-state synthesis of ZnS/graphene nanocomposites with enhanced photocatalytic activity. *Dyes and Pigments* **2015,** *120*, 8-14.

21. Huang, X.; Willinger, M. G.; Fan, H.; Xie, Z. L.; Wang, L.; Klein-Hoffmann, A.; Girgsdies, F.; Lee, C. S.; Meng, X. M., Single crystalline wurtzite ZnO/zinc blende ZnS coaxial heterojunctions and hollow zinc blende ZnS nanotubes: synthesis, structural characterization and optical properties. *Nanoscale* **2014,** *6* (15), 8787-95.

22. Golsheikh, A. M.; Lim, H. N.; Zakaria, R.; Huang, N. M., Sonochemical synthesis of reduced graphene oxide uniformly decorated with hierarchical ZnS nanospheres and its enhanced photocatalytic activities. *RSC Adv.* **2015,** *5* (17), 12726-12735.

23. Hong, E.; Kim, J. H., Oxide content optimized ZnS–ZnO heterostructures via facile thermal treatment process for enhanced photocatalytic hydrogen production. *International Journal of Hydrogen Energy* **2014,** *39* (19), 9985-9993.

24. Peng, T.; Li, K.; Zeng, P.; Zhang, Q.; Zhang, X., Enhanced Photocatalytic Hydrogen Production over Graphene Oxide–Cadmium Sulfide Nanocomposite under Visible Light Irradiation. *The Journal of Physical Chemistry C* **2012,** *116* (43), 22720-22726.

25. Mondal, C.; Singh, A.; Sahoo, R.; Sasmal, A. K.; Negishi, Y.; Pal, T., Preformed ZnS nanoflower prompted evolution of CuS/ZnS p–n heterojunctions for exceptional visible-light driven photocatalytic activity. *New J. Chem.* **2015,** *39* (7), 5628-5635.

26. Zhang, J.; Yu, J.; Zhang, Y.; Li, Q.; Gong, J. R., Visible light photocatalytic H(2)-production activity of CuS/ZnS porous nanosheets based on photoinduced interfacial charge transfer. *Nano letters* **2011,** *11* (11), 4774-9.

27. Wang, X.; Li, Y.; Wang, M.; Li, W.; Chen, M.; Zhao, Y., Synthesis of tunable ZnS–CuS microspheres and visible-light photoactivity for rhodamine B. *New Journal of Chemistry* **2014,** *38* (9), 4182.

28. Yu, J.; Zhang, J.; Liu, S., Ion-Exchange Synthesis and Enhanced Visible-Light Photoactivity of CuS/ZnS Nanocomposite Hollow Spheres. *Journal of Physical Chemistry C* **2010,** *114* (32), 13642-13649.

29. Thuy, U. T. D.; Liem, N. Q.; Parlett, C. M. A.; Lalev, G. M.; Wilson, K., Synthesis of CuS and CuS/ZnS core/shell nanocrystals for photocatalytic degradation of dyes under visible light. *Catalysis Communications* **2014,** *44*, 62-67.

30. Feng, C.; Zhang, L.; Wang, Z.; Song, X.; Sun, K.; Wu, F.; Liu, G., Synthesis of copper sulfide nanowire bundles in a mixed solvent as a cathode material for lithium-ion batteries. *Journal of Power Sources* **2014,** *269*, 550-555.

31. Zhang, S.; Li, J.; Wang, X.; Huang, Y.; Zeng, M.; Xu, J., Rationally designed 1D Ag@AgVO3nanowire/graphene/protonated g-C3N4nanosheet heterojunctions for enhanced photocatalysis via electrostatic self-assembly and photochemical reduction methods. *J. Mater. Chem. A* **2015,** *3* (18), 10119-10126.

32. Zhang, L. J.; Xie, T. F.; Wang, D. J.; Li, S.; Wang, L. L.; Chen, L. P.; Lu, Y. C., Noble-metal-free CuS/CdS composites for photocatalytic H 2 evolution and its photogenerated charge transfer properties. *International Journal of Hydrogen Energy* **2013,** *38* (27), 11811-11817.

33. Feng, C.; Zhang, L.; Yang, M.; Song, X.; Zhao, H.; Jia, Z.; Sun, K.; Liu, G., One-Pot Synthesis of Copper Sulfide Nanowires/Reduced Graphene Oxide Nanocomposites with Excellent Lithium-Storage Properties as Anode Materials for Lithium-Ion Batteries. *ACS applied materials & interfaces* **2015,** *7* (29), 15726-34.

34. Wang, Q.; Yun, G.; Bai, Y.; An, N.; Chen, Y.; Wang, R.; Lei, Z.; Shangguan, W., CuS, NiS as co-catalyst for enhanced photocatalytic hydrogen evolution over TiO2. *International Journal of Hydrogen Energy* **2014,** *39* (25), 13421-13428.

35. Lee, M.; Yong, K., Highly efficient visible light photocatalysis of novel CuS/ZnO heterostructure nanowire arrays. *Nanotechnology* **2012,** *23* (19), 194014.

36. Yu, J. G.; Zhang, J.; Liu, S. W., Ion-Exchange Synthesis and Enhanced Visible-Light Photoactivity of CuS/ZnS Nanocomposite Hollow Spheres. *J. Phys. Chem. C* **2010,** *114* (32), 13642-13649.

37. Zhang, L. J.; Xie, T. F.; Wang, D. J.; Li, S.; Wang, L. L.; Chen, L. P.; Lu, Y. C., Noble-metal-free CuS/CdS composites for photocatalytic H2 evolution and its photogenerated charge transfer properties. *International Journal of Hydrogen Energy* **2013,** *38* (27), 11811-11817.

38. Sing, K. S. W., Reporting physisorption data for gas/solid systems with special reference to the determination of surface area and porosity (Recommendations 1984). *Pure & Applied Chemistry* **2009,** *57* (11), 603-619.

39. Cheng, J.; Yan, H.; Lu, Y.; Qiu, K.; Hou, X.; Xu, J.; Han, L.; Liu, X.; Kim, J.-K.; Luo, Y., Mesoporous CuCo2O4nanograsses as multi-functional electrodes for supercapacitors and electro-catalysts. *J. Mater. Chem. A* **2015,** *3* (18), 9769-9776.

40. Han, Y.; Wu, X.; Ma, Y.; Gong, L.; Qu, F.; Fan, H., Porous SnO2 nanowire bundles for photocatalyst and Li ion battery applications. *CrystEngComm* **2011,** *13* (10), 3506.

41. Sinha, A. K.; Manna, P. K.; Pradhan, M.; Mondal, C.; Yusuf, S. M.; Pal, T., Tin oxide with a p–n heterojunction ensures both UV and visible light photocatalytic activity. *RSC Adv.* **2014,** *4* (1), 208-211.

42. Xiaoxiao, Y.; Jiaguo, Y.; Bei, C.; Baibiao, H., One-pot template-free synthesis of monodisperse zinc sulfide hollow spheres and their photocatalytic properties. *Chemistry (Weinheim an der Bergstrasse, Germany)* **2009,** *15* (27), 6731-6739.

43. Qiu, X.; Miyauchi, M.; Yu, H.; Irie, H.; Hashimoto, K., Visible-light-driven Cu(II)-(Sr(1-y)Na(y))(Ti(1-x)Mo(x))O3 photocatalysts based on conduction band control and surface ion modification. *Journal of the American Chemical Society* **2010,** *132* (43), 15259-67.

44. Yu, H.; Irie, H.; Hashimoto, K., Conduction Band Energy Level Control of Titanium Dioxide: Toward an Efficient Visible-Light-Sensitive Photocatalyst. *Journal of the American Chemical Society* **2010,** *132* (20), 6898-6899.

45. Irie, H.; Kamiya, K.; Shibanuma, T.; Miura, S.; Tryk, D. A.; Yokoyama, T.; Hashimoto, K., Visible Light-Sensitive Cu(II)-Grafted TiO2 Photocatalysts: Activities and X-ray Absorption Fine Structure Analyses. *J. Phys. Chem. C* **2009,** *113* (24), 10761-10766.

46. Hong, Y.; Zhang, J.; Huang, F.; Zhang, J.; Wang, X.; Wu, Z.; Lin, Z.; Yu, J., Enhanced visible light photocatalytic hydrogen production activity of CuS/ZnS nanoflower spheres. *J. Mater. Chem. A* **2015,** *3* (26), 13913-13919.

47. Li, K.; Chen, R.; Li, S.-L.; Han, M.; Xie, S.-L.; Bao, J.-C.; Dai, Z.-H.; Lan, Y.-Q., Self-assembly of a mesoporous ZnS/mediating interface/CdS heterostructure with enhanced visible-light hydrogen-production activity and excellent stability. *Chem. Sci.* **2015,** *6* (9), 5263-5268.

48. Khanchandani, S.; Kumar, S.; Ganguli, A. K., Comparative Study of TiO2/CuS Core/Shell and Composite Nanostructures for Efficient Visible Light Photocatalysis. *ACS Sustainable Chemistry & Engineering* **2016,** *4* (3), 1487-1499.

49. Sungjee, K.; Brent, F.; Hans-Jürgen, E.; Moungi, B., Type-II quantum dots: CdTe/CdSe(core/shell) and CdSe/ZnTe(core/shell) heterostructures. *Journal of the American Chemical Society* **2003,** *125* (38), 11466-7.